Inorganic Chemistry

ARTICLE

pubs.acs.org/IC

Solid-State Photoluminescence Sensitization of Tb^{3+} by Novel Au_2Pt_2 and Au_2Pt_4 Cyanide Clusters

LeAnn Ladner,[†] Tu Ngo,[†] Carlos Crawford,[‡] Zerihun Assefa,*[,‡] and Richard E. Sykora*[,†]

[†]Department of Chemistry, University of South Alabama, Mobile, Alabama 36688, United States

[‡]Department of Chemistry, North Carolina A&T State University, Greensboro, North Carolina 27411, United States

Supporting Information

ABSTRACT: The syntheses are reported for two novel Tb^{3+} heterotrimetallic cyanometallates, $K_2[Tb(H_2O)_4(Pt(CN)_4)_2]$-$Au(CN)_2 \cdot 2H_2O$ (**1**) and $[Tb(C_{10}N_2H_8)(H_2O)_4(Pt(CN)_4)$-$(Au(CN)_2)] \cdot 1.5C_{10}N_2H_8 \cdot 2H_2O$ (**2**) ($C_{10}N_2H_8$ = 2,2′-bipyridine). Both compounds have been isolated as colorless crystals, and single-crystal X-ray diffraction has been used to investigate their structural features. Crystallographic data (Mo$K\alpha$, λ = 0.71073 Å, T = 290 K): **1**, tetragonal, space group $P4_2/nnm$, a = 11.9706(2) Å, c = 17.8224(3) Å, V = 2553.85(7) Å^3, Z = 4; **2**, triclinic, space group $P\bar{1}$, a = 10.0646(2) Å, b = 10.7649(2) Å, c = 17.6655(3) Å, α = 101.410(2)°, β = 92.067(2)°, γ = 91.196(2)°, V = 1874.14(6) Å^3, Z = 2. For the case of **1**, the structure contains Au_2Pt_4 hexameric noble metal clusters, while **2** includes Au_2Pt_2 tetrameric clusters. The clusters are alike in that they contain Au−Au and Au−Pt, but not Pt−Pt, metallophilic interactions. Also, the discrete clusters are directly coordinated to Tb^{3+} and sensitize its emission in both solid-state compounds, **1** and **2**. The Photoluminescence (PL) spectra of **1** show broad excitation bands corresponding to donor groups when monitored at the Tb^{3+} ion f-f transitions, which is typical of donor/acceptor energy transfer (ET) behavior in the system. The compound also displays a broad emission band at ∼445 nm, assignable to a donor metal centered (MC) emission of the Au_2Pt_4 clusters. The PL properties of **2** show a similar Tb^{3+} emission in the visible region and a lack of donor-based emission at room temperature; however, at 77 K a weak, broad emission occurs at 400 nm, indicative of uncoordinated 2,2′-bipyridine, along with strong Tb^{3+} transitions. The absolute quantum yield (QY) for the Tb^{3+} emission ($^5D_4 \rightarrow {}^7F_{J\,(J=6-3)}$) in **1** is 16.3% with a lifetime of 616 μs when excited at 325 nm. In contrast the weak MC emission at 445 nm has a quantum yield of 0.9% with a significantly shorter lifetime of 0.61 μs. For **2** the QY value decreases to 9.3% with a slightly shorter lifetime of 562 μs. The reduced QY in **2** is considered to be a consequence of (1) the slightly increased donor−acceptor excited energy gap relative to the optimal gap suggested for Tb^{3+} and (2) Tb^{3+} emission quenching via a bpy ligand-to-metal charge transfer (LMCT) excited state.

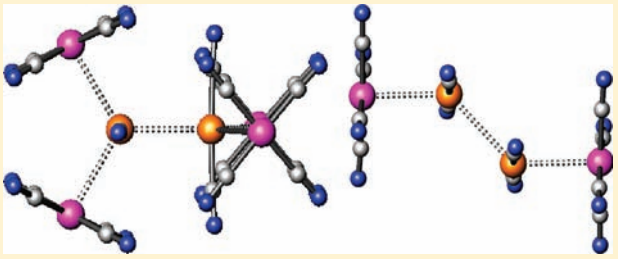

INTRODUCTION

The importance of metal containing polymers for new materials is quite extensive, and Au(I) and Pt(II) based compounds are of particular importance because of their interesting physical and chemical properties.[1−3] In this regard, cyanide-bridged heterometallic systems, prepared by assembling cyanometallates, for example, $[Au(CN)_2]^-$ or $[Pt(CN)_4]^{2-}$, and transition metal or lanthanide ions exhibit fascinating structural, birefringent, luminescent, and catalytic properties.[3−8] In such compounds, aurophilic (Au−Au) and platinophilic (Pt−Pt) interactions are prominent examples of a more general phenomenon of metallophilicity, which is recognized as a major force determining structural dimensionality and properties.[4,9]

It has been well established that lanthanide tetracyanoplatinates typically contain platinophilic interactions in a chain-like fashion whereby the square planar $[Pt(CN)_4]^{2-}$ anions stack in a parallel fashion in close proximity in their solid-state structures.[7,10] This type of arrangement is observed, for example in $Ln_2[Pt(CN)_4]_3 \cdot 21H_2O$ (Ln = Tb−Yb).[7,10,11] The linear $[Au(CN)_2]^-$ anion has been used to construct a family of lanthanide dicyanoaurates, $Ln[Au(CN)_2]_3 \cdot 3H_2O$ (Ln = La−Dy),[8] that contain two-dimensional (2-D), kagome-type layers constructed from aurophilic interactions. Both lanthanide dicyanoaurate and tetracyanoplatinate compounds (Ln-$[Au(CN)_2]_3 \cdot 3H_2O$ (Ln = La,[8a] Eu,[8b] Tb[8c]), $Ln_2[Pt(CN)_4]_3 \cdot xH_2O$ (Ln = La−Yb),[12−14] etc.) have been extensively studied for a number of years, mainly in regards to their interesting luminescence properties. It has been shown that donor $[Au(CN)_2]^-$ can sensitize Tb^{3+} luminescence in both solids[8c,8d] and solutions.[15] The latter studies proposed that the energy transfer (ET) process can occur from donor excimers or exciplexes formed from $[Au(CN)_2^-]_n$ oligomers[16] to the Tb^{3+} acceptors.[15]

In recent years, transition-metal complexes suitable for use as chromophores have gained increasing interest as sensitizers of lanthanide ion acceptors.[17−19] A major advantage afforded by these chromophores is their ability to sustain a better energy match-up with

Received: September 7, 2010
Published: February 09, 2011

   dx.doi.org/10.1021/ic101836a | *Inorg. Chem.* 2011, 50, 2199–2206

most Ln^{3+} acceptor states.[13,17,20−22] Unique advantages of these metal complexes over organic chromophores are that they provide a relatively high triplet quantum yield because of the rapid intersystem crossing inherent within the system (because of the heavy-atom effect), and the possibility of a facile detection of both quenching of the d-block chromophores and the sensitized emission from the lanthanide centers.[23−29] On the basis of these known results and the previous work mentioned above on lanthanide cyanometallates we set out to (1) prepare novel lanthanide *heterotrimetallic* cyanides that incorporate both $[Au(CN)_2]^-$ and $[Pt(CN)_4]^{2-}$ and contain Au−Pt interactions, (2) determine the structural characteristics of these heterometallic interactions, and (3) investigate the possibility of using these novel heterometallic systems as sensitizers for select Ln^{3+} cations.

In this study, the coordination of the $Au(CN)_2^-$ and $Pt(CN)_4^{2-}$ anions to the Tb^{3+} centers has been conducted in a rational approach to explore our current interest,[30] namely, the spectroscopic processes of a dual donor effect in sensitized emission. In compound **1**, $K_2[Tb(H_2O)_4(Pt(CN)_4)_2]Au(CN)_2\cdot 2H_2O$, the two metallic anions, $[Pt(CN)_4]^{2-}$ and $[Au(CN)_2]^-$, are assembled and collectively coordinated to the Tb^{3+} ion. This compound allowed us to first explore whether such heterobimetallic units can be used as sensitizers for the Tb^{3+} ions. Compound **2**, $[Tb(C_{10}N_2H_8)(H_2O)_4(Pt(CN)_4)(Au(CN)_2)]\cdot 1.5C_{10}N_2H_8\cdot 2H_2O$, was synthesized with an additional bidentate ligating 2,2′-bipyridine ligand coordinated to the Tb^{3+} center. The procedure has allowed us to conduct a step by step comparison of multi donor effects in these systems. Structural characterizations of **1** and **2** have revealed the presence of $[(Au(CN)_2)_2(Pt(CN)_4)_4]^{10-}$ and $[(Au(CN)_2)_2(Pt(CN)_4)_2]^{6-}$ clusters, respectively, which can also be described as hexameric and tetrameric oligomers. These particular discrete *heterobimetallic* moieties, which sport Au−Pt and Au−Au interactions, are unique features to these two compounds. The structures and photoluminescence properties of both novel, *heterotrimetallic* Tb^{3+} cyanometallates are described in greater detail herein.

EXPERIMENTAL SECTION

Materials and Methods. $Tb(CF_3SO_3)_3\cdot 9H_2O$ (Aldrich, 98%), $K_2[Pt(CN)_4]\cdot 3H_2O$ (Alfa Aesar, 99.9%), $K[Au(CN)_2]$ (Alfa Aesar, 99.99%), and 2,2′-bipyridine (Alfa Aesar, 99%) were used as received without further purification. IR spectra were obtained on neat crystalline samples at room temperature (RT) using a Jasco FT/IR-4100 with a diamond ATR attachment in the range 4000−650 cm^{-1}. CHN analyses were performed by Galbraith Laboratories, Inc. in Knoxville, TN.

*Synthesis of $K_2[Tb(H_2O)_4(Pt(CN)_4)_2]Au(CN)_2\cdot 2H_2O$ (**1**).* **1** was prepared in 86% yield from $Tb(CF_3SO_3)_3$, $K_2[Pt(CN)_4]$, and $K[Au(CN)_2]$ in a 1:4 mixture of H_2O:CH_3CN. The reaction was conducted in a 5 mL test tube by preparing and mixing the three following solutions: 1 mL of 0.10 M $Tb(CF_3SO_3)_3\cdot 9H_2O$ (4:1 CH_3CN:H_2O), 1 mL of 0.15 M $K_2[Pt(CN)_4]\cdot 3H_2O$ (4:1 CH_3CN:H_2O), and 1 mL of 0.10 M $KAu(CN)_2$ (4:1 CH_3CN:H_2O). Slow evaporation of the solvent resulted in a harvest of colorless crystals of **1** after approximately one week. IR (solid, cm^{-1}): 3628 (w), 3556 (w), 3350 (m,br), 3224 (m,br), 2189 (w), 2170(m), 2144 (s), 2133 (s), 1662 (w), 1633 (m). Elemental Analysis: Calculated for $C_{10}H_{12}AuK_2N_{10}O_6Pt_2Tb$: C, 10.07; H, 1.01; N, 11.75. Found: C, 10.10; H, 1.07; N, 11.35.

*Synthesis of $[Tb(C_{10}N_2H_8)(H_2O)_4(Pt(CN)_4)(Au(CN)_2)]\cdot 1.5C_{10}N_2H_8\cdot 2H_2O$ (**2**).* **2** was synthesized in 50% yield from $Tb(CF_3SO_3)_3$, $K_2[Pt(CN)_4]$, $K[Au(CN)_2]$, and 2,2′-bipyridine in a 1:9 mixture of EtOH:H_2O. The reaction was conducted in a 5 mL test tube by preparing and mixing the four following solutions: 1 mL of 0.10 M $Tb(CF_3SO_3)\cdot 9H_2O$ (aq), 1 mL of 0.15 M $K_2[Pt(CN)_4]\cdot 3H_2O$ (aq), 1 mL of 0.10 M $KAu(CN)_2$ (aq), and 1.5 mL of 0.067 M 2,2′-bipyridine (1:2 EtOH:H_2O). Evaporation of the solvent over a period of several days resulted in the crystallization of **2** as colorless single crystals. IR (solid, cm^{-1}): 3556 (w), 3394 (m,br), 3209 (m,br), 3099 (m,br), 2178 (m), 2153 (s), 2128 (s), 1653 (m), 1634 (m), 1595 (s), 1574 (m), 1493 (m), 1476 (m), 1464 (m), 1437 (s), 1428 (m,sh), 1317 (m), 1260 (w), 1248 (w), 1224 (w), 1176 (w), 1158 (m), 1119 (w), 1098 (w), 1067 (w), 1045 (w), 1011 (s), 969 (w), 815 (w), 760 (s), 736 (s). Elemental Analysis: Calculated for $C_{31}H_{32}AuN_{11}O_6PtTb$: C, 30.89; H, 2.68; N, 12.78. Found: C, 30.78; H, 2.79; N, 12.66.

Table 1. Crystallographic Data for $K_2[Tb(H_2O)_4(Pt(CN)_4)_2]$-$Au(CN)_2\cdot 2H_2O$ (1) and $[Tb(C_{10}N_2H_8)(H_2O)_4(Pt(CN)_4)$-$(Au(CN)_2)]\cdot 1.5C_{10}N_2H_8\cdot 2H_2O$ (2)

	1	2
formula	$C_{10}H_{12}AuK_2N_{10}$-O_6Pt_2Tb	$C_{31}H_{32}AuN_{11}$-O_6PtTb
formula weight (amu)	1192.56	1205.65
space group	$P4_2/nnm$ (No. 134)	$P\bar{1}$ (No. 2)
a (Å)	11.9706(2)	10.0646(2)
b (Å)	11.9706(2)	10.7649(2)
c (Å)	17.8224(3)	17.6655(3)
α (deg)	90	101.410(2)
β deg)	90	92.067(2)
γ (deg)	90	91.196(2)
V (Å^3)	2553.85(7)	1874.14(6)
Z	4	2
T (K)	290	290
λ (Å)	0.71073	0.71073
ρ_{calcd} (g cm^{-3})	3.102	2.136
μ(Mo Kα) (mm^{-1})	19.753	9.550
$R(F_o)$ for $F_o^2 > 2\sigma(F_o^2)$[a]	0.0185	0.0227
$R_w(F_o^2)$[b]	0.0438	0.0548

[a] $R(F_o) = \sum||F_o|-|F_c||/\sum|F_o|$. [b] $R_w(F_o^2) = [\sum[w(F_o^2-F_c^2)^2]/\sum wF_c^4]^{1/2}$.

Single-Crystal X-ray Diffraction. Single crystals of **1** and **2** were selected, mounted on quartz fibers, and aligned with a digital camera on a Varian Oxford Xcalibur E single-crystal X-ray diffractometer. Intensity measurements were performed using Mo Kα radiation, from a sealed-tube Enhance X-ray source, and an Eos area detector. CrysAlisPro[31] was used for preliminary determination of the cell constants, data collection strategy, and for data collection control. Following data collection, CrysAlisPro was also used to integrate the reflection intensities, apply an absorption correction to the data, and perform a global cell refinement.

Crystals of **1** and **2** diffracted extremely well and were not problematic in regards to structure solution and refinement. For both structure analyses, the program suite SHELX was used for structure solution (XS) and least-squares refinement (XL).[32] The initial structure solutions were carried out using direct methods, and the remaining heavy atom positions were located in difference maps. The final refinements included anisotropic displacement parameters for all non-hydrogen atoms and isotropic refinements for all H positions. Refinement was performed against F^2 by weighted full-matrix least-squares and empirical absorption corrections (SADABS) were applied. Crystal data for **1** and **2** is included in Table 1 and additional crystallographic details are available as Supporting Information. Data can also be obtained free of charge in cif format by request from The Cambridge Crystallographic Data Centre at www.ccdc.cam.ac.uk/data_request/cif with the CCDC numbers 777449 and 777450 for **1** and **2**, respectively.

Photoluminescence (PL) Measurements. The PL spectra were collected using a Photon Technology International (PTI) spectrometer (model QM-7/SE). The system uses a high intensity (150 W) xenon source for excitation. Selection of excitation and emission wavelengths are conducted

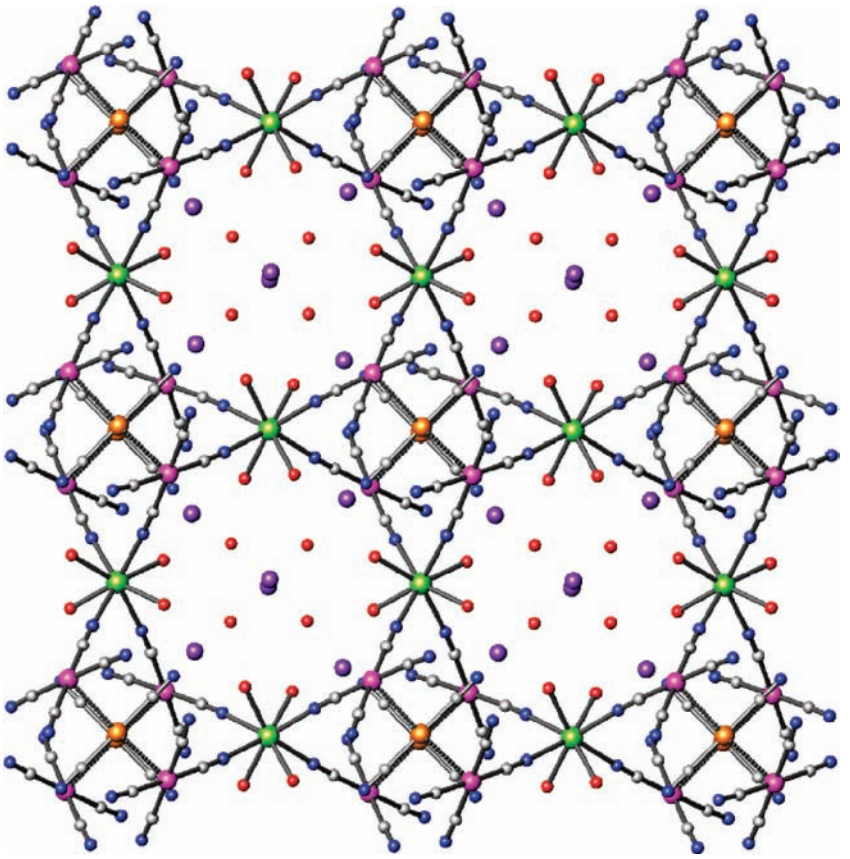

Figure 1. Representation of the 2-D structure in **1** viewed along the *c* axis. Color scheme: Tb in green, Pt in pink, Au in orange, K in purple, C in gray, N in blue, and O in red.

by means of computer controlled, autocalibrated "QuadraScopic" monochromators and are equipped with aberration corrected emission and excitation optics. Signal detection is accomplished with a PMT detector (model 928 tube) that can work either in analog or digital (photon counting) modes. Emission spectra are corrected by an established methodology. The instrument operation, data collection, and handling were all controlled using the advanced FeliX32 fluorescence spectroscopic package.

For the lifetime measurements, an Advanced TimeMaster fluorescence and phosphorescence system with "QuadraScopic" monochromators and PMT and laser Strobe (PTI TM3) detectors was used. With dual detectors, the system is capable of lifetime measurements in the range of picoseconds to seconds. Time-resolved measurements are routinely conducted on the system. Various time delays were introduced ranging from 40−120 μs for the Tb^{3+} emission of **1** and **2**, and 2−10 μs for the donor (Au−Pt based) emission of **1**. All of the spectroscopic experiments were conducted on neat crystalline samples held in sealed quartz capillary tubes, and the 77 K measurements were conducted on the same samples inserted in a coldfinger dewar filled with liquid nitrogen.

The absolute PL quantum yield (QY) measurements on the solids were conducted using a PTI QM-40, PLQY ultrasensitive fluorimeter system containing a 6-in. integrating sphere (K-Sphere B) redesigned for enhanced measurement of quantum yields of solids, films, and powders. The system includes dedicated quantum yield calculation functions. Wavelength selection is conducted by software controlled excitation and emission monochromators. The QY measurements were conducted on finely ground solids uniformly spread onto the sample holder and covered with a quartz disk.

RESULTS AND DISCUSSION

Structural Studies. The structure of **1** consists of 2-D $[Tb(H_2O)_4(Pt(CN)_4)_2]^-$ layers formed by the linkage of the Tb^{3+} cations by cis-bridging tetracyanoplatinate anions to four additional Tb^{3+} cations as shown in Figure 1. This arrangement results in 24-member rings with pores that are occupied by K^+ cations and waters of hydration. The 2-D layers stack in a fashion (Supporting Information, Figures S1−S4) as to preclude the formation of extended channels throughout the structure. The $[Au(CN)_2]^-$ anions are not coordinated directly to the Tb^{3+} site in the structure; rather they are locked in the structure by a combination of Au−Au aurophilic (3.1953(8) Å) and Au−Pt heterometallophilic (3.2658(3) Å) interactions. These interactions result in the formation of $[(Au(CN)_2)_2(Pt(CN)_4)_4]^{10-}$ (Au_2Pt_4) hexameric clusters with D_{2d} symmetry, shown in Figure 2. The distorted square antiprismatic coordination environment of the Tb^{3+} cations are completed by four coordinated water molecules. The Tb−N, Tb−O, Pt−C, and Au−C bond distances are presented in Table 2 and are quite ordinary.[8,10,11]

The structure of **2** contains a reduced structural dimensionality relative to **1** as a result of the chelating ancillary ligand, 2,2′-bipyridine (bpy); whereas **1** is a 2-D coordination polymer, **2** is a molecular complex as seen in the thermal ellipsoid plot presented in Figure 3. This is a trend that we have also observed in previous work on lanthanide tetracyanoplatinate systems[30,33] whereby chelating cyclic amines coordinate Ln^{3+} cations, effectively reducing the number of bridging ligands (tetracyanoplatinate) present on the 4f-element cations. In **2**, the coordination sphere of each Tb^{3+} cation contains one bidentate bpy, four coordinated water molecules, one N-bound $[Pt(CN)_4]^{2-}$, and one N-bound $[Au(CN)_2]^-$ anion, unlike in **1** where the $[Au(CN)_2]^-$ was uncoordinated. Crystallized between these neutral $[Tb(C_{10}N_2H_8)(H_2O)_4(Pt(CN)_4)(Au(CN)_2)]$ complexes are additional uncoordinated bpy and water

dx.doi.org/10.1021/ic101836a |*Inorg. Chem.* 2011, 50, 2199–2206

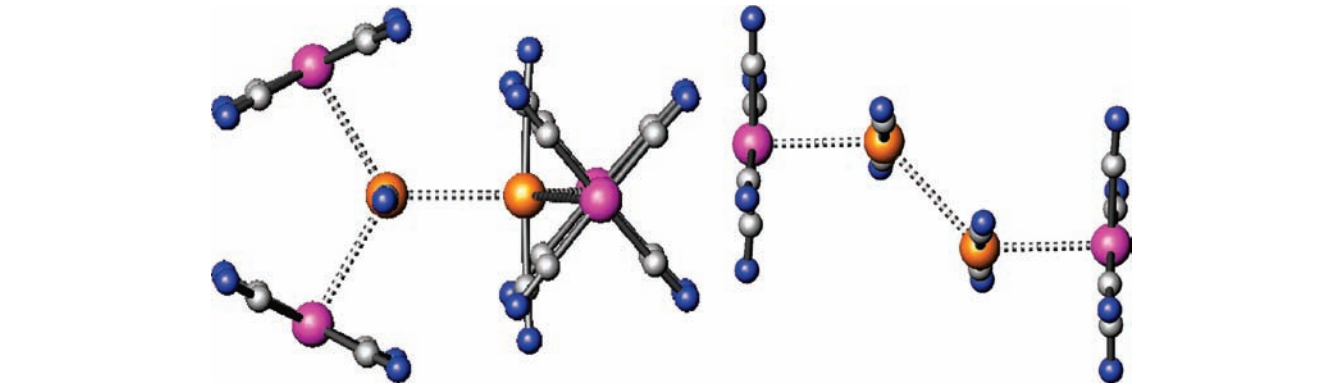

Figure 2. Left: Au_2Pt_4 hexameric clusters in **1**. Right: Au_2Pt_2 tetrameric clusters in **2**. The dashed lines indicate metallophilic interactions.

Table 2. Selected Bond Distances (Å) for $K_2[Tb(H_2O)_4(Pt(CN)_4)_2]Au(CN)_2 \cdot 2H_2O$ (1)

Tb1−O1	2.394(3)	C1−N1	1.135(6)
Tb1−N1	2.460(4)	C2−N2	1.151(6)
Pt1−C1	1.987(5)	C3−N3	1.150(9)
Pt1−C2	1.978(5)	Au1−Au1[a]	3.1953(8)
Au1−C3	1.981(8)	Au1−Pt1	3.2658(3)
Tb1−Tb1[a]	8.4645(8)		

[a] Symmetry transformation used to generate equivalent atoms: $y + 1/2$, $-x + 1$, $-z + 1/2$.

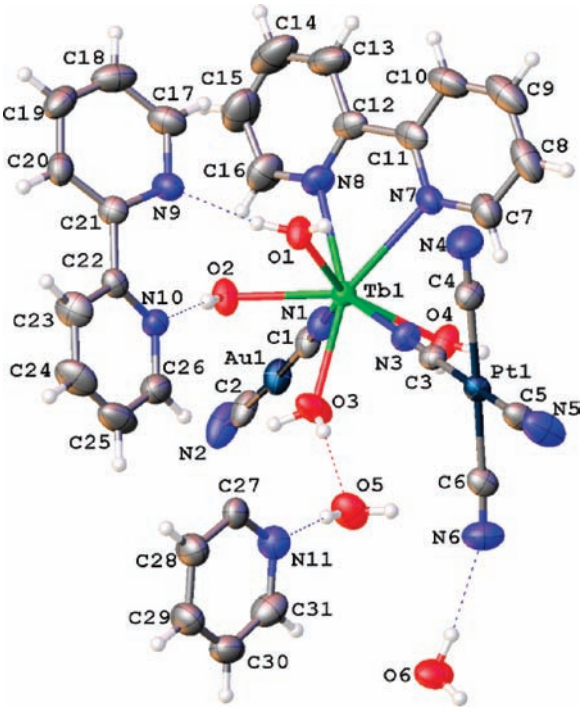

Figure 3. Thermal ellipsoid plot (50%), with atom labeling scheme, of the asymmetric unit in **2**.

molecules. Select bond distances for the Tb1, Pt1, and Au1 coordination environments in **2** are included in Table 3.

Interestingly, four metal complexes in **2** arrange in such a fashion (Supporting Information, Figure S5) as to form $[(Au(CN)_2)_2(Pt(CN)_4)_2]^{6-}$ (Au_2Pt_2) tetrameric clusters (C_{2h} symmetry), shown in

Table 3. Selected Bond Distances (Å) for $[Tb(C_{10}N_2H_8)(H_2O)_4(Pt(CN)_4)(Au(CN)_2)] \cdot 1.5C_{10}N_2H_8 \cdot 2H_2O$ (2)

Tb1−O1	2.334(3)	Au1−C1	1.981(4)
Tb1−O2	2.362(3)	Au1−C2	1.990(5)
Tb1−O3	2.365(3)	C1−N1	1.134(5)
Tb1−O4	2.385(3)	C2−N2	1.124(5)
Tb1−N1	2.474(4)	C3−N3	1.144(5)
Tb1−N3	2.457(3)	C4−N4	1.141(6)
Tb1−N7	2.552(4)	C5−N5	1.133(6)
Tb1−N8	2.549(4)	C6−N6	1.139(6)
Pt1−C3	1.981(4)	Au1−Au1[a]	3.3123(4)
Pt1−C4	1.993(5)	Au1−Pt1[b]	3.1987(3)
Pt1−C5	1.991(5)	Tb1−Tb1[c]	8.1682(4)
Pt1−C6	1.991(5)		

[a] Symmetry transformations used to generate equivalent atoms: $-x + 1$, $-y + 2$, $-z$. [b] Symmetry transformations used to generate equivalent atoms: x, $y + 1$, z. [c] Symmetry transformations used to generate equivalent atoms: $-x + 2$, $-y + 1$, $-z$.

Figure 2, that contain both Au−Au aurophilic (3.3123(4) Å) and Au−Pt heterometallophilic (3.1987(3) Å) interactions. Therefore, the structures of **1** and **2** reveal the absence of both 1-D noble-metal chains and 2-D kagome sheets which dominate the chemistry of lanthanide tetracyanoplatinates[7,10,11] and dicyanoaurates,[8] respectively. While several reports have noted the formation of small metal moieties containing Au−Pt heterometallic interactions,[9,34,35] these distinct Au_2Pt_4 and Au_2Pt_2 clusters in **1** an **2**, respectively, are quite novel. Further, we believe compounds **1** and **2** to be the first examples where a Ln^{3+} cation has been complexed by Au−Pt heterometallic clusters.

Photoluminescence Studies. The RT emission and excitation spectra of **1** are shown in Figure 4. Excitation at 337, 400, or 420 nm results in similar emission profiles where a weak, broad-band is centered at ~445 nm and a series of stronger sharp bands representing the emission of the Tb^{3+} ion ($^5D_4 \rightarrow {}^7F_J$ ($J = 0-6$) transitions) are present. The broad band is uncharacteristic of Tb^{3+} emission and can be assigned to Au_2Pt_4 emission based on the sub microsecond lifetime and similar energy position and profile compared with other compounds exhibiting Au−Pt based emission.[34]

The room-temperature excitation spectrum observed using 543 nm emission contains two intense, broad bands with maxima at 325 and 420 nm and a shoulder at 399 nm (Figure 4). Additionally, a poorly resolved shoulder appears on the higher energy side of the 325 nm band and a weak doublet of sharp bands appears with

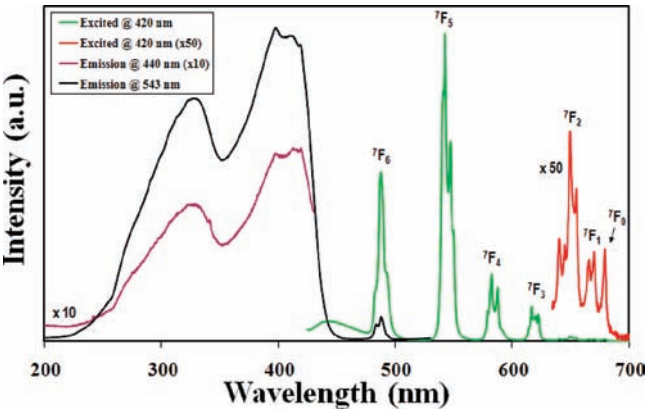

Figure 4. Room temperature PL spectra of **1**. The excitation was monitored at 543 nm Tb^{3+} emission (black) and 440 nm Au_2Pt_4 emission (purple; ×10). The emission spectrum was collected upon excitation at 420 nm (green; red ×50). Similar emission profiles are also observed upon excitation at 337 or 400 nm. The initial state for the Tb^{3+} emission is $^5D_4$ and the terminal $^{2S+1}L_J$ multiplets are labeled.

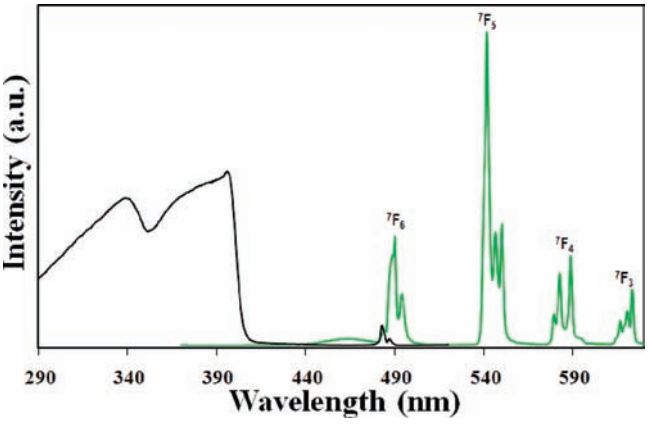

Figure 5. Low temperature (77 K) PL spectra for **1**. The excitation was monitored at 543 nm Tb^{3+} emission (black) and the emission was collected upon excitation at 420 nm (green). The initial state for the Tb^{3+} emission is $^5D_4$ and the terminal $^{2S+1}L_J$ multiplets are labeled.

maxima at 484 and 488 nm. The latter, sharp bands are characteristic of the Tb^{3+} ion $^5D_4 \leftarrow {}^7F_6$ absorption band, while the broad higher energy bands are assigned to Au_2Pt_4 (MC) based excitations.

The excitation spectrum of **1** measured at 77 K and monitored at the 543 nm band has two broad band regions centered at ∼340 and ∼398 nm, which drops sharply between 400 and 418 nm as shown in Figure 5. Excitation into either the 340 or the 398 nm band provides characteristic Tb^{3+} f-f lines in addition to a weak broad band that maximizes at 465 nm. The broad band emission in the 77 K spectrum is red-shifted by ∼20 nm (∼1000 cm^{-1}) when compared with the RT spectrum. Similar RT excitation profiles are obtained when monitored either at the broad Au_2Pt_4 or the Tb^{3+} emission as can be seen in Figure 4. This finding is a direct evidence of ET in this system, where the sensitized emission is achieved through ET from the Au_2Pt_4 donor moiety to the acceptor Tb^{3+} ion.

Comparison of the emission intensities of the Tb^{3+} ion $^5D_4 \rightarrow {}^7F_5$ transition in **1** reveals that at RT the band is ∼4 times more intense than at 77 K, for an otherwise identical instrumental setup, indicating that a higher quantum efficiency is exhibited at RT. Temperature dependent M−M expansion and a concomitant blue

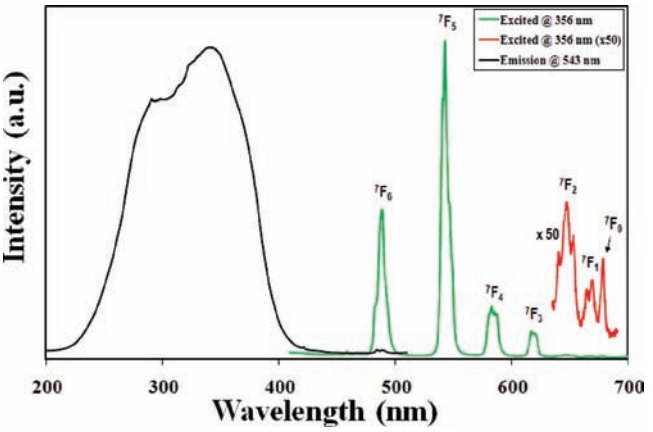

Figure 6. Room temperature PL spectra for **2**. The excitation was monitored at 543 nm Tb^{3+} emission (black). The emission spectrum was collected upon excitation at 356 nm (green; red ×50). For the Tb^{3+} emission, the initial state is $^5D_4$ and the terminal $^{2S+1}L_J$ multiplets are labeled.

shift of the emission bands is a well-known phenomenon in Pt and Au photochemistry,[1] and hence the low temperature red shift (20 nm relative to RT) of the Au_2Pt_4 cluster emission is believed to arise from slight changes in intermetallic interactions. The efficiency increase is related to the blue shift of the donor band at RT creating a nearly nominal gap between the donor and the $^5D_4$ emitting states. Commonly accepted excitation mechanisms of lanthanide ions involve the population of lanthanide f-f emitting states via ET from the sensitizer ligand triplet states, which themselves are populated by intersystem crossing (ISC) from the ligand singlet states initially excited by photons or electrons.[25,26,28,29,36] Hence the overall efficiency of the sensitized emission is directly related with the intersystem-crossing and the energy-transfer efficiencies. One factor that is known to affect the efficiency of the ET step is the position of the donor triplet state relative to the emitting $^5D_4$ state of the Tb^{3+} ion. Assuming the position of the $^5D_4$ state to be 20500 cm^{-1}, the gap between the donor and the emitting Tb^{3+} states is ∼2000 versus 1000 cm^{-1} at RT and 77 K, respectively, for compound **1**. Compared with the nominal gap suggested by Latva et al.[37] it is evident that the radiative efficiency at RT should be larger than at 77 K as has been observed here.

In contrast, the influence of the structural changes in **2**, relative to **1**, on the PL profiles are clearly evident in Figures 6−8. The excitation profile (543 nm emission) measured at RT for **2** clearly lacks the lower energy broad band present in the spectrum of **1**; hence, the two compounds have drastically different excitation profiles as seen in Figure 8. The lowest energy excitation band in **2** is blue-shifted by ∼40 nm in comparison to **1** and is more likely related to the longer aurophilic interaction in **2** (longer by 0.117 Å). Excitation into this broad band provides characteristic green Tb^{3+} emission for **2** as shown in Figure 6. Moreover, donor emission from **2** is entirely absent in the RT data (excitation at 325 nm). However, a weak, broad band appears at 400 nm when measured at 77 K (Figure 7). The overall excitation profiles of **2** at RT and 77 K are essentially unchanged, although a sharper shoulder is distinct at 77 K.

Comparison of the excitation spectra for the two complexes is shown in Figure 8. At first glance, the lack of the donor Au_2Pt_2 emission at RT may imply a complete transfer of energy to the Tb^{3+} cation. If that were the case one would anticipate a concomitant increase in the emission intensity from the donor. It may also mean that a non-radiative process in the Au_2Pt_2 donor may compete with the ET processes even at low temperatures since efficient non-radiative

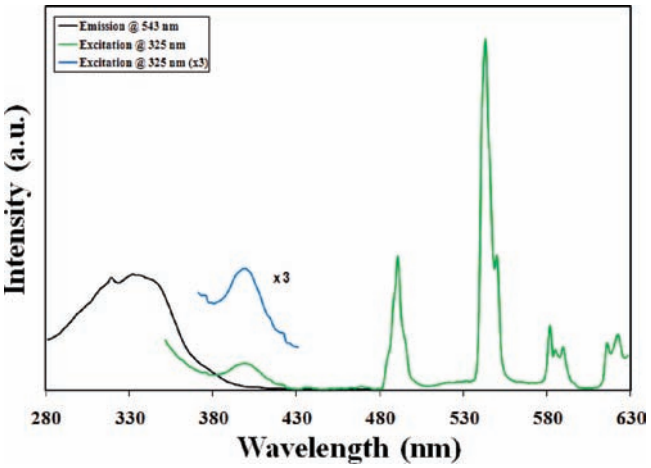

Figure 7. Low temperature (77 K) PL spectra for **2**. The excitation was monitored at 543 nm Tb^{3+} emission (black), and the emission was collected upon excitation at 325 nm (green; blue ×3). The weak broad band at 400 nm is assigned as emission from the uncoordinated 2,2′-bipyridine in the lattice.

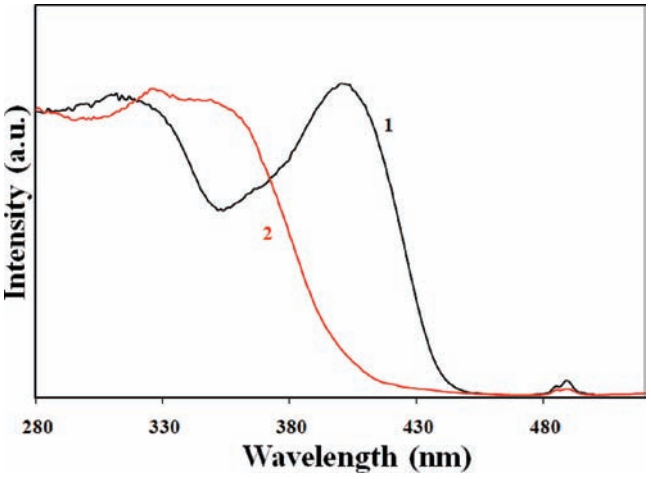

Figure 8. Comparison of excitation spectra for **1** (black) and **2** (red). Both spectra were collected by monitoring Tb^{3+} emission (543 nm).

processes restricting emission have been previously noted in similar systems such as in $[Pt(L)_2][Au(CN)_2]_2$ (L = en, bpy).[35] Hence, quantum yield measurements were found important in discerning the overall processes in these systems.

Quantum Yield (QY) Studies. The overall QY for the Tb^{3+} emissions of **1** is 16.3% upon excitation at 325 nm. The lifetime measured at the most intense band ($^5D_4 \rightarrow {}^7F_5$; 543 nm) is 616 μs. In contrast, the weak Au_2Pt_4 MC emission at 445 nm has a quantum yield value of 0.9% and a significantly shorter lifetime of 0.61 μs. For compound **2**, the Tb^{3+} emission ($^5D_4 \rightarrow {}^7F_5$; 543 nm) has a slightly shorter lifetime of 562 μs, and the overall QY value decreases to 9.3%. On the basis of these values, the radiative and non-radiative rate constants, k_r and k_{nr}, respectively, were calculated[38] using eqs 1 and 2 and the results presented in Table 4:

$$k_r = \frac{\phi_{sp}}{\tau_{obs}} \quad (1)$$

$$k_{nr} = \left(\frac{1}{\tau_{obs}} - k_r\right) \quad (2)$$

where, ϕ_{sp} is the quantum yield and τ_{obs} is the measured lifetime.

Table 4. Luminescence and Photophysical Data for 1 and 2

compound	ϕ_{sp}	τ, μs	k_r, s^{-1}	k_{nr}/k_{ET}, s^{-1}
1[a]	0.163	616	2.65×10^2	1.36×10^3
1[b]	0.009	0.61	1.47×10^4	1.62×10^6
2[b]	0.093	562	1.65×10^2	1.61×10^3

[a] Lifetime data correspond to the 543 nm Tb^{3+} emission, while QY data correspond to the $^5D_4 \rightarrow {}^7F_{J\ (J=6-3)}$ Tb^{3+} f−f emission bands. [b] Data correspond to the 445 nm donor emission.

Estimate of the ET rate in compound **1** was possible due to the observance of the weak MC emission. Assuming ET as the dominant non-radiative decay step for the MC de-excitation, a rate constant of 1.62×10^6 s^{-1} is estimated as the upper limit for the ET (k_{ET}) path in **1**. Although the lack of donor emission at RT in **2** precluded comparison of the ET rates, the radiative rate constant in compound **2** is only ∼60% of that of **1** (Table 4).

The significant blue shift expected in the Au/Pt-based donor state of **2** (as a result of expansion in the Au−Au interaction) as compared with that of **1** is consistent with the report by Latva et al.[37] that the quantum yield in Tb^{3+} will be weak if the triplet donor state is located out of the optimal range. The empirical rule developed by them suggests that an optimal donor-to-metal ET is attainable when the energy gap between the donor triplet state and the acceptor f-state of the Tb^{3+} ion ($\Delta E(^3T-{}^5D_4)$), is between 2500−4500 cm^{-1}.[37] The energy gap in **1** is ∼2100 cm^{-1}, slightly out of the suggested range. Hence, structural fine-tuning in these compounds is necessary to create ideal conditions for increased efficiency of the ET process.

Although it is tempting to assign the high energy broad emission (400 nm) of **2** as a donor (MC) band, the combined spectral features of this band warrants an alternative assignment. First, the band is observed only at low temperatures. Second, excitation dependency of this emission is clearly evident in that the 400 nm emission is observed only upon exciting the higher energy side of the excitation band shown for **2** (Figure 8). Slowly increasing the excitation wavelength from 300 nm upward results in increasing emission intensity until a maximum is reached at ∼318 nm and then slowly decreases thereafter. At an excitation wavelength of 350 nm, the 400 nm band is totally absent at both RT and 77 K. The excitation spectrum shows a sharp component at ∼318 nm (Figure 7) overlaying on top of the broad excitation band, where the maximum emission intensity is observed. Both the sharp excitation band and the position of the broad emission at 400 nm are consistent with the reported PL profile for the free 2,2′-bipyridine ligand.

Bekiari et al.[39] have reported that free bpy ligand in poly(ethyleneglycol) solution has a weak emission band that maximizes at 396 nm. Comparison of this spectral profile with that of **2** suggests that the broad emission band at ∼400 nm can be assigned to the uncoordinated bpy ligand present in the lattice. The fact that the 400 nm band shows a unique dependency on the excitation wavelength, different from that of the acceptor Tb^{3+} emission, indicates a lack of donor−acceptor type spectral coupling between the free bpy and the Tb^{3+} emission. In this regard the uncoordinated bpy is not expected to have a strong contribution in enhancing the emission from **2**. However, the weakness of the band intensity at 400 nm combined with an inability to conduct lifetime measurements at temperatures lower than 77 K has limited the opportunity to discern the band more closely.

However, the coordinated bpy can very likely be involved in the establishment of a ligand-to-metal charge transfer (LMCT) excited state. Since the effects of such states in reducing the

dx.doi.org/10.1021/ic101836a |*Inorg. Chem.* 2011, 50, 2199–2206

radiative efficiencies have been noted earlier[39−43] in bpy-containing lanthanide complexes, a similar situation could also occur in **2**. Overall, the results indicate that the role of the bpy ligand in enhancing the Tb^{3+} emission from **2** is minimal or negative, relative to **1**, because of the larger energy gap between the $^3\pi\pi^*$ state of bpy (triplet state at 288 nm) and the acceptor $^5D_4$ level, as well as possible formation of a LMCT state that may contribute in the quenching of the emission.

SUMMARY AND CONCLUSIONS

Synthesis and solid-state structural studies of two novel Tb^{3+} heterotrimetallic cyanometallates, $K_2[Tb(H_2O)_4(Pt(CN)_4)_2]Au(CN)_2\cdot 2H_2O$ (**1**) and $[Tb(C_{10}N_2H_8)(H_2O)_4(Pt(CN)_4)(Au(CN)_2)]\cdot 1.5C_{10}N_2H_8\cdot 2H_2O$ (**2**), are presented. These compounds have both been shown to contain discrete noble-metal oligomers (clusters); compound **1** contains $[(Au(CN)_2)_2(Pt(CN)_4)_4]^{10-}$ (Au_2Pt_4) oligomers while **2** contains $[(Au(CN)_2)_2(Pt(CN)_4)_2]^{6-}$ (Au_2Pt_2) oligomers. Sensitized luminescence of Tb^{3+} cations has been observed to occur via either cluster in the solid state. These moieties represent a possible link between the long-range 2-D aurophilic and 1-D platinophilic substructures in the solid-state compounds, $Tb[Au(CN)_2]_3\cdot 3H_2O$ and $Tb_2[Pt(CN)_4]_3\cdot 21H_2O$, and the small metal cyanide oligomers that have been observed in previous solution studies. The PL spectra of **1** show an intense characteristic emission of the Tb^{3+} ion f-f transitions upon donor based excitation indicating a typical donor/acceptor ET behavior in the compound. The Tb^{3+} emission in **1** contains an absolute QY of 16.3% and a lifetime of 616 μs. At RT a weak donor emission is also observed at 445 nm, but red shifts to 465 nm at 77 K. This weak MC emission has a quantum yield of 0.9% with a significantly shorter lifetime of 0.61 μs, relative to the Tb^{3+} emission in **1**. The red shift at low temperature is associated with a reduced Au−Au interaction that lowers the gap between the highest occupied molecular orbital (HOMO) and the lowest unoccupied molecular orbital (LUMO) in this system. The PL properties of **2** show a similar Tb^{3+} emission in the visible region and a lack of donor-based emission at RT; however, at 77 K a weak emission, presumably from uncoordinated bpy, occurs at 400 nm along with strong Tb^{3+} emission. For **2**, the QY value decreases to 9.3% with a slightly shorter lifetime of 562 μs. The reduced QY in **2** is likely a consequence of (1) the slightly increased donor−acceptor excited energy gap relative to the optimal gap suggested for Tb^{3+} and (2) the Tb^{3+} emission quenching via a LMCT excited state.

ASSOCIATED CONTENT

Supporting Information. X-ray crystallographic data for **1** and **2** in CIF format and additional structural figures and photoluminescence data. This material is available free of charge via the Internet at http://pubs.acs.org.

AUTHOR INFORMATION

Corresponding Author

*E-mail: rsykora@jaguar1.usouthal.edu (R.E.S.), zassefa@ncat.edu (Z.A.). Phone: 1 (251) 460-7422 (R.E.S.), 1 (336) 285-2255 (Z.A.).

ACKNOWLEDGMENT

The authors gratefully acknowledge the National Science Foundation for their generous support (NSF-CAREER, CHE-0846680). Z.A. acknowledges support from NOAA-EPP award no. NA06OAR48101187, and the donors of the ACS-PRF. The collection of the X-ray data for **2** was performed by Milorad Stojanovic.

REFERENCES

(1) Forward, J. M.; Fackler, J. P., Jr.; Assefa, Z. In *Optoelectronic Properties of Inorganic Compounds*; Roundhill, D. M., Fackler, J. P., Jr., Eds.; Plenum Press: New York, 1999; pp 195−229.
(2) Yam, V. W.-W.; Wong, K. M.-C.; Zhu, N. *J. Am. Chem. Soc.* 2002, *124*, 6506–6507.
(3) Katz, M. J.; Kaluarachi, H.; Batchelor, R. J.; Bokov, A. A.; Ye, Z.-G.; Leznoff, D. B. *Angew. Chem., Int. Ed.* 2007, *46*, 8804–8807.
(4) Leznoff, D. B.; Xue, B.-Y.; Patrick, B. O.; Sanchez, V.; Thompson, R. C. *Chem. Commun.* 2001, 259–260.
(5) Katz, M. J.; Ramnial, T.; Yu, H.-Z.; Leznoff, D. B. *J. Am. Chem. Soc.* 2008, *130*, 10662–10673.
(6) Jujjuri, S.; Ding, E.; Shore, S. G.; Keane, M. A. *J. Mol. Catal. A: Chem.* 2007, *272*, 96–107.
(7) Gliemann, G.; Yersin, H. *Struct. Bonding (Berlin)* 1985, *62*, 87–153, and references therein.
(8) (a) Colis, J. C. F.; Larochelle, C.; Staples, R.; Herbst-Irmer, R.; Patterson, H. *Dalton Trans.* 2005, 675–679. (b) Assefa, Z.; Shankle, G.; Patterson, H. H.; Reynolds, R. *Inorg. Chem.* 1994, *33*, 2187–2195. (c) Tanner, P. A.; Zhou, X.; Wong, W.-T.; Kratzer, C.; Yersin, H. *J. Phys. Chem. B* 2005, *109*, 13083–13090. (d) Rawashdeh-Omary, M. A.; Larochelle, C. L.; Patterson, H. H. *Inorg. Chem.* 2000, *39*, 4527–4534. (e) Assefa, Z.; Kalachnikova, K.; Haire, R. G.; Sykora, R. E. *J. Solid State Chem.* 2007, *180*, 3121–3129.
(9) Fernández, E. J.; Laguan, A.; López-de-Luzuriaga, J. M. *Dalton Trans.* 2007, 1969–1981, and references therein.
(10) Holzapfel, W.; Yersin, H.; Gliemann, G. *Z. Kristallogr.* 1981, *157*, 47–67, and references therein.
(11) Loosli, A.; Wermuth, M.; Güdel, H.-U.; Capelli, S.; Hauser, J.; Bürgi, H.-B. *Inorg. Chem.* 2000, *39*, 2289–2293.
(12) Daniels, W.; Yersin, H.; Philipsborn, H.v.; Gliemann, G. *Solid State Commun.* 1979, *30*, 353–355.
(13) Yersin, H.; von Ammon, W.; Stock, M.; Gliemann, G. *J. Lumin.* 1979, *18−19*, 774–778.
(14) Yersin, H.; Stock, M. *J. Chem. Phys.* 1982, *76*, 2136–2138.
(15) Guo, Z.; Yson, R. L.; Patterson, H. H. *Chem. Phys. Lett.* 2007, *445*, 340–344.
(16) Rawashdeh-Omary, M. A.; Omary, M. A.; Patterson, H. H.; Fackler, J. P., Jr. *J. Am. Chem. Soc.* 2001, *123*, 11237–11247.
(17) Klink, S. I.; Keizer, H.; Van Veggel, F. C. J. M. *Angew. Chem., Int. Ed.* 2000, *39*, 4319–4321.
(18) Shavaleev, N. M.; Moorcraft, L. P.; Pope, S. J. A.; Bell, Z. R.; Faulkner, S.; Ward, M. D. *Chem. Commun.* 2003, 1134–1135.
(19) Shavaleev, N. M.; Accorsi, G.; Virgili, D.; Bell, Z. R.; Lazarides, T.; Calogero, G.; Armaroli, N.; Ward, M. D. *Inorg. Chem.* 2005, *44*, 61–72.
(20) Beltyukova, S. V.; Tselik, E. I.; Egorova, A. V. *J. Pharm. Biomed. Anal.* 1998, *18*, 261–266.
(21) Panigrahi, B. S.; Peter, S.; Viswanathan, K. S.; Mathews, C. K. *Spectrochim. Acta A* 1995, *51A*, 2289–2300.
(22) Zhao, G.; Zhao, S.; Gao, J.; Kang, J.; Yang, W. *Talanta* 1997, *45*, 303–307.
(23) Zang, F. X.; Hong, Z. R.; Li, W. L.; Li, M. T.; Sun, X. Y. *Appl. Phys. Lett.* 2004, *84*, 2679–2681.
(24) Bünzli, J.-C. G.; Piguet, C. *Chem. Soc. Rev.* 2005, *34*, 1048–1077.
(25) Xu, H.-B.; Shi, L.-X.; Ma, E.; Zhang, L.-Y.; Wei, Q.-H.; Chen, Z.-N. *Chem. Commun.* 2006, 1601–1603.
(26) Guo, D.; Duan, C.-Y.; Lu, F.; Hasegawa, Y.; Meng, Q.-J.; Yanagida, S. *Chem. Commun.* 2004, 1486–1487.
(27) Li, X.-L.; Dai, F.-R.; Zhang, L.-Y.; Zhu, Y.-M.; Peng, Q.; Chen, Z.-N. *Organometallics* 2007, *26*, 4483–4490.
(28) Daws, C. A.; Exstrom, C. L.; Sowa, J. R., Jr.; Mann, K. R. *Chem. Mater.* 1997, *9*, 363–368.

(29) Baca, S. G.; Pope, S. J. A.; Adams, H.; Ward, M. D. *Inorg. Chem.* 2008, *47*, 3736–3747.
(30) (a) Maynard, B. A.; Smith, P. A.; Ladner, L.; Jaleel, A.; Beedoe, N.; Crawford, C.; Assefa, Z.; Sykora, R. E. *Inorg. Chem.* 2009, *48*, 6425–6435. (b) Maynard, B. A.; Kalachnikova, K.; Whitehead, K.; Assefa, Z.; Sykora, R. E. *Inorg. Chem.* 2008, *47*, 1895–1897. (c) Maynard, B. A.; Smith, P. A.; Jaleel, A.; Ladner, L.; Sykora, R. E. *J. Chem. Crystallogr.* 2010, *40*, 616–623.
(31) *Xcalibur CCD system, CrysAlisPro Software system*, Version 1.171.33; Oxford Diffraction Ltd.: Abingdon, U.K., 2010.
(32) Sheldrick, G. M. *Acta Crystallogr.* 2008, *A64*, 112–122.
(33) Stojanovic, M.; Robinson, N. J.; Chen, X.; Smith, P. A.; Sykora, R. E. *J. Solid State Chem.* 2010, *183*, 933–939.
(34) Stender, M.; White-Morris, R. L.; Olmstead, M. M.; Balch, A. L. *Inorg. Chem.* 2003, *42*, 4504–4506.
(35) Stork, J. R.; Pham, D.; Bicocca, V.; Olmstead, M. M.; Balch, A. L. *Inorg. Chem.* 2005, *44*, 3466–3472.
(36) Bünzli, J-C. G.; Comby, S.; Chauvin, A.-S.; Vandevyver, C. D. B. *Rare-Earths* 2007, *25*, 257–274.
(37) Latva, M.; Takalo, H.; Mukkala, V.-M.; Matachescu, C.; Rodriguez-Ubis, J. C.; Kankare, J. *J. Lumin.* 1997, *75*, 149–169.
(38) (a) Quici, S.; Marzanni, G.; Cavazzini, M.; Anelli, P. L.; Botta, M.; Gianolio, E.; Accorsi, G.; Armaroli, N.; Barigelletti, F. *Inorg. Chem.* 2002, *41*, 2777–2784. (b) Gao, X.-C.; Cao, H.; Huang, C.-H.; Umitani, S.; Chen, G.-Q.; Jiang, P. *Synth. Met.* 1999, *9*, 127–132.
(39) Bekiari, V.; Pistolis, G.; Lianos, P. *Chem. Mater.* 1999, *11*, 3189–3195.
(40) Lis, S.; Elbanowski, M.; Akowska, B. M.; Hnatejko, Z. *J. Photochem. Photobiol., A* 2002, *150*, 233–247.
(41) Sabbatini, N.; Guardigli, M.; Lehn, J. M. *Coord. Chem. Rev.* 1993, *123*, 201–228.
(42) Binnemans, K. In *Handbook on the Physics and Chemistry of the Rare Earths*; Gschneidner, K. A., Bünzli, J.-C., Pecharsky, V. K., Eds.; Elsevier/North Holland: New York, 2005; Vol. 35, pp 107−272.
(43) Weissman, S. I. *J. Chem. Phys.* 1942, *10*, 214–217.